EQUALIZED MULTI-STEP STRESSING OF POST-TENSIONING TENDONS OF CYLINDRICAL SHELLS: A CASE STUDY

By

MAURIZIO LENZI AND PAOLA CAMPANA

POST-TENSIONING INSTITUTE ®

Authorized reprint from: AUGUST 2013 issue of the PTI Journal

EQUALIZED MULTI-STEP STRESSING OF POST-TENSIONING TENDONS OF CYLINDRICAL SHELLS: A CASE STUDY

BY MAURIZIO LENZI AND PAOLA CAMPANA

The equalized step-by-step post-tensioning of cylindrical-shell water tanks and silos is analyzed in this paper. The study shows that, as a consequence of the friction reactions that arise along the circular tendons, only a part of the total length of the strands really contributes to the elongations of the tendons during the post-tensioning steps. This fact significantly affects the distribution of the axial forces along the tendons and the stretching of the strands, whose monitoring is required during tensioning. The validation of the model is based on the comparison between the theoretical elongations of the tendons with the experimental values recorded during the equalized multi-step stressing of post-tensioning tendons of a cylindrical silo built for the storage of the clinker inside the port of Ravenna, Italy. The agreement of the results in this case study is satisfactory.

RESEARCH SIGNIFICANCE

The objective of the research is to deduce, based on a consistent number of measures, a criterion able to explain the behavior of the post-tensioned curvilinear tendons. The results show that in the multi-step stressing of post-tensioning tendons, the distribution of the axial forces and the tendon elongations are independent of the load increments, and depend instead on the position of the inversion point in the direction of the friction forces.

KEYWORDS

Equalized prestressing; friction loss; inversion point; multi-step post-tensioning; tendon elongation.

PTI JOURNAL, V. 9, No. 1, August 2013. Received and reviewed under Institute journal publication policies. Pertinent discussion will be published in the next issue of *PTI JOURNAL* if received within 3 months of the publication.

INTRODUCTION

In post-tensioned structures with large prestressing forces and tendon deviation causing large friction losses, it is common to apply the prestressing following a step-by-step procedure to introduce the forces gradually. This is done by alternating the stressing several times on both ends of the tendons. Compared with the case of the force applied in a single step, the distribution of the axial force and of the strain in the tendons in the multi-step procedure is not always simple to evaluate, especially regarding the influence of the friction losses. The prestress transferred to the structure is in fact affected by the slip resistance of the tensioned strands, which varies along the circular path of the tendon. The friction forces that act on the strand are in an opposite direction to the displacement of the strand in the current stressing step. They invert directions during the next stressing step when prestressing force is applied from the opposite end. This peculiar feature of the friction implies that the effects of the stressing steps cannot be simply added up. The value of the friction forces depend not only on the total value of the applied prestressing force in that section of the tendon but also on the direction of the strand displacement induced in the current stressing step. That implies that, during the post-tensioning operation, the elongated part of the tendon changes, varying the influence distance of the applied force at the live end anchor. This fact produces interesting consequences that are illustrated in the paper.

FRICTION REACTION ALONG TENDONS

The equilibrating forces that act on an infinitesimal length of tendon are shown in Fig. 1. Due to the contact pressure p exerted by the strands against the duct and to the slip, δ, of the strands, the tendon is subjected to a friction force equal to[1]

$$t = \mu \cdot p = \mu \cdot N/R \qquad (1)$$

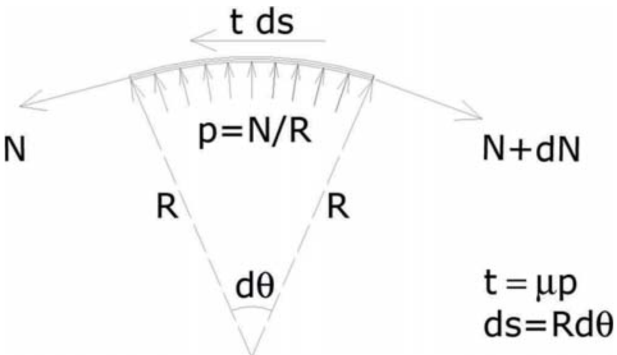

Fig. 1—Equilibrium of infinitesimal length of tendon.

This friction force is proportional to the friction coefficient μ, to the axial force N, and to the curvature $1/R$ of the tendon, where R is the local radius of the shell. The correlation t-δ between the friction force and the slip (Fig. 2), shown by the dashed line, that is associated with the bond behavior of the contact, has a very high stiffness. The reaction increases up to the force that induces the first movement. Once the slippage has occurred, the friction reaction is then assumed to remain almost constant for all the values of the slip.[2]

ANALYSIS OF BALANCED CONFIGURATION OF CIRCULAR TENDON

The behavior of the tendons in the balanced configuration is considered in which the tendon is stressed with a force N_L at the left edge and a force N_R at the right edge, as shown in Fig. 3. Such an analysis introduces the basic concepts that will be used when dealing with the case of the step-by-step post-tensioning. In a balanced configuration with simultaneous tensioning, the strand stretches on both the sides respectively in the direction of the applied force. The axial force along the tendon decreases as a consequence of the friction between the strands and the duct. It follows that in a balanced configuration of the tendon, an inversion point must exist where the displacement of the strand is null and where the axial force on the left side of the inversion point must equal the axial force acting at the right side of that point. It thus divides the tendon in two parts. In each part, the strands are stretched in the direction of the applied force according to the following scheme. Indicated as dN—the increment of the axial force varying the arc length of an infinitesimal segment ds—the balance of the axial forces requires

$$dN \pm t \cdot ds = 0 \tag{2}$$

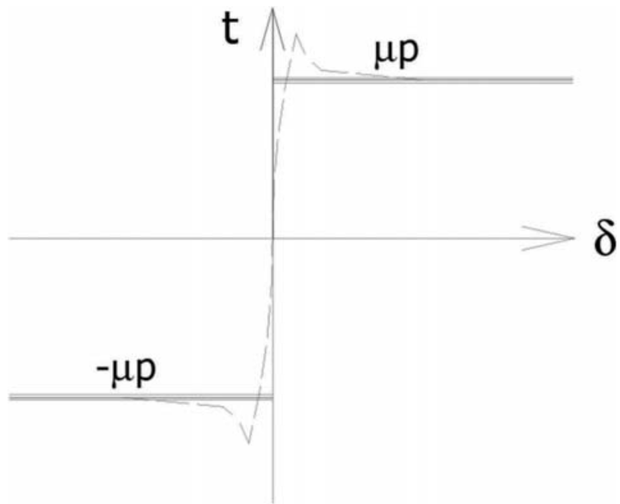

Fig. 2—Relation between friction and slip.

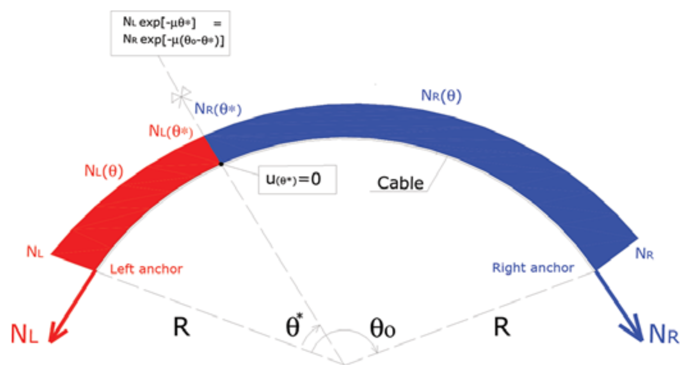

Fig. 3—Balanced configuration of circular post-tensioned tendon.

The sign of the friction force depends on the direction of the elongation of the strand, with the positive sign valid for the left side and the negative sign for the right side of the tendon. The current point along the tendon is denoted by θ. Making use of the relation $ds = R{\cdot}d\theta$, the previous differential balance equation then becomes

$$\frac{dN}{d\vartheta} \pm \mu \cdot N = 0 \tag{3}$$

This relationship shows that the distribution of the axial force in the tendon does not depend on the radius of curvature of the tendon but only on the friction coefficient and on the values of the axial forces at the ends of the tendon. This represents the boundary conditions of the homogenous differential equation.

With θ_o being the angular width of the tendon, the integration provides these equations that give the distribution of axial forces along the tendon

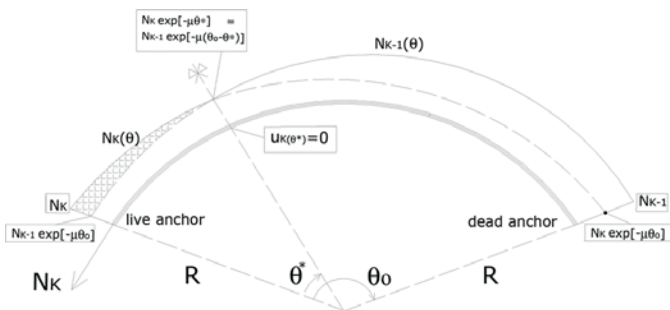

Fig. 4—Axial forces in tendon in current post-tensioning step.

$$N_L(\vartheta) = N_L \cdot e^{-\mu\vartheta} \quad 0 \le \theta \le \theta^* \tag{4}$$

$$N_R(\vartheta) = N_R \cdot e^{-\mu(\vartheta_o - \vartheta)} \quad \theta^* \le \theta \le \theta_o \tag{5}$$

The symbol θ^* represents the angle of the inversion point where the axial displacement $u(\theta^*)$ of the tendon is zero. This point can be found by imposing the equilibrium condition $N_L(\theta^*) = N_R(\theta^*)$ that, written extensively, becomes

$$N_L \cdot e^{-\mu\vartheta^*} = N_R \cdot e^{-\mu(\vartheta_o - \vartheta^*)} \tag{6}$$

It thus provides

$$\vartheta^* = \frac{1}{2}\left[\vartheta_o + \frac{1}{\mu} Ln \frac{N_L}{N_R}\right] \quad [0 \le \vartheta^* \le \vartheta_o] \tag{7}$$

This angle identifies an axis of symmetry for the arc whose angular width is $2\theta^*$—the location where the axial force reaches its minimum and the location where the directions of the friction forces are opposite. Once the position of the inversion point is identified, the total elongation of the tendon can be evaluated as the sum of the elongations of the two stretched segments by means of the relation

$$\Delta L_{tot} = \int_0^{\vartheta^*} \frac{N_L(\vartheta)}{EA} R \cdot d\vartheta + \int_{\vartheta^*}^{\vartheta_o} \frac{N_R(\vartheta)}{EA} R \cdot d\vartheta \tag{8}$$

It shows that in the case of circular tendons, the elongation of the tendons is proportional to the term R/EA and to the area of the diagram representing the distribution of the axial forces.

STEP-BY-STEP POST-TENSIONING

A step-by-step procedure is usually followed in post-tensioning stressing operations when the prestressing force to be applied to the structures is large. In such a case, tendons are stressed by alternating from one end to the other. This procedure is called multi-step post-tensioning. The analysis shows that in the case of the step-by-step post-tensioning, the final distribution of the axial forces along the tendon is the same as the case in which the total force is applied simultaneously in a single step. The analysis previously shown establishes, in the range of validity of the basic assumptions, what follows. *The equilibrated configuration of the tendon is uniquely defined by the values of the tensioning forces at the two ends of the tendon. In other words, the distribution of the axial forces along the tendon is independent of the number of the steps by means of which the values of the final forces are reached.* The same result is also valid for the elastic potential energy stored in the strands, on which the elongation of the tendon depends.

As a consequence, *the total cumulative elongation of the tendon is the same as the simultaneous tensioning case.* Also, the elongation of the tendon during the current post-tensioning step can be simply computed as the difference between the total elongation in the current tensioning step and that observed in the previous one. It corresponds, by the term R/EA, to the shaded area of the diagram of the axial force distribution illustrated in Fig. 4. This diagram also shows that *the length of the tendon that is stretched during the current tensioning step always runs from the live end anchor to the inversion point.*

In step-by-step post-tensioning, it is useful to follow the variation of the position of the inversion point. To this purpose, it is convenient to denote N_K as the force applied to the live end anchor in the current step and N_{K-1} as the force applied at the opposite block in the previous tensioning step. As an example, the case of the complete inversion of the friction forces will now be considered while the more general case will be shown later in the paper. The angle that defines the position of the inversion point may vary between two limits—$\theta^* = 0$ and $\theta^* = \theta_o$—which are reached for the following values of the prestressing force

$$\vartheta^* = 0 \text{ when } N_K \le N_{K-1} \cdot e^{-\mu\vartheta_o}$$
$$\text{(conical wedges releasing)} \tag{9}$$

$$\vartheta^* = \vartheta_o/2 \text{ when } N_K = N_{K-1}$$
$$\text{(symmetry of axial force distribution)} \tag{10}$$

$$\vartheta^* = \vartheta_o \text{ when } N_K \geq N_{K-1} \cdot e^{+\mu\vartheta_o} \quad (11)$$
(complete inversion of friction forces)

In the current step of the post-tensioning, a force greater than the force induced in the previous tensioning step must be applied to release the conical wedges and to start to stretch the strands ($\theta^* = 0$). As the jacking force increases, the length of the reacting segment grows, extending as far as the current inversion point. Beyond this point, no slip occurs between the strands and the duct, and the axial force in the tendon remains "frozen" at the values induced by the previous post-tensioning step. As the force is further increased, a symmetric (equalized) configuration of the axial forces is reached ($\theta^* = \theta_o/2$). Increasing the tensioning force even more may result in a complete inversion of the direction of the friction forces ($\theta^* = \theta_o$).

EQUALIZED POST-TENSIONING

It is of interest to consider the recurring case in which the applied forces at the jack are brought to the same level at both the ends, acting first from one block and then from the other one. This operation is denoted as the *equalization of the prestressing forces*. At the end of this sequence, the maximum value of the axial force in the tendon, N_K, is reached at both ends while the minimum value, equal to $N_K \cdot e^{-\mu\theta_o/2}$, is reached in the center of the tendon in the same way as the tensioning would be if stressed from both ends simultaneously up to the total value of the force from both the ends in a single step. At the end of k-th equalized step, the total elongation of the tendon is thus equal to

$$\Delta L_{K,eq.tot} = 2\int_0^{\vartheta_o/2} \frac{N_K \cdot e^{-\mu\vartheta}}{EA} \cdot R \cdot d\vartheta \quad (12)$$

SUMMARY OF MULTI-STEP POST-TENSIONING PROCEDURE

The measurement of elongations of the tendons and comparing them to the theoretical values is one of the basic control measures to take place during the post-tensioning operations. The evaluation of the theoretical elongations is summarized for the more general case.

1. In the k-th tensioning step, one denotes $N_T = N_K$ as the applied force at the live end anchor and N_F is the reaction induced in the fixed end anchor. The reaction N_F is equal to the maximum of the value N_{K-1}, which is the force applied in the previous step (which happens when a high friction prevents the complete elongation of the strand and always when the end forces are equalized), and the value $N_K \cdot e^{-\mu\theta_o}$ (which is reached at the fixed end anchor when there is complete inversion of the friction forces along the tendon, as it always happens in the first tensioning step). Thus, one assumes

$$N_T = N_K \text{ (at the live end anchor)} \quad (13)$$

$$N_F = \max\{N_{K-1},\, N_K \cdot e^{-\mu\vartheta_o}\} \text{ (at the dead end anchor)} \quad (14)$$

2. The angle θ^*, which defines the location of the inversion point, is

$$\vartheta^* = \frac{1}{2}\left[\vartheta_o + \frac{1}{\mu} Ln\frac{N_L}{N_R}\right][0 \leq \vartheta^* \leq \vartheta_o] \quad (15)$$

where N_L and N_R are the forces applied at the left end anchor and at the right end anchor, which assign each time the values N_T and N_F previously defined.

3. The total elongation of the tendon is computed as the sum of the elongations of the two parts on either side of the inversion point. For a circular tendon, the lengths of those arcs are $L_L = R\theta^*$ for the left side and $L_R = R(\theta_o - \theta^*)$ for the right side, respectively, so that the total elongation becomes

$$\Delta L_{K,tot} = \frac{N_L L_L}{EA}\left[\frac{1-e^{-\mu\vartheta^*}}{\mu\vartheta^*}\right] + \frac{N_R L_R}{EA}\left[\frac{1-e^{-\mu(\vartheta_o-\vartheta^*)}}{\mu(\vartheta_o-\vartheta^*)}\right] \quad (16)$$

Each one of the two contributions is given by the elastic elongation of the tendon computed as if no friction would act, reduced by means of a coefficient (that appears inside the brackets) that accounts for the influence of the friction losses.[3] It can be noted that when the complete inversion of the direction of the friction forces occurs (which is the case in which $\theta^* = 0$ or $\theta^* = \theta_o$), all the segments of the tendon are stretched in the same direction and they all contribute to the elongation of the tendon. The fixed end anchor provides the reaction that grants the equilibrium. This occurs when the force N_K, applied at the live end anchor, reaches the value $N_{K-1} \cdot e^{+\mu\theta_o}$. Beyond this point, the elongation of the tendon increases in proportion to the applied force (linear correlation) because the inversion

Fig. 5—Clinker silo cylindrical shell. (Note: R = 56.6 ft [17.25 m]; H = 105 ft [32 m]; and b = 13.8 in. [35 cm].)

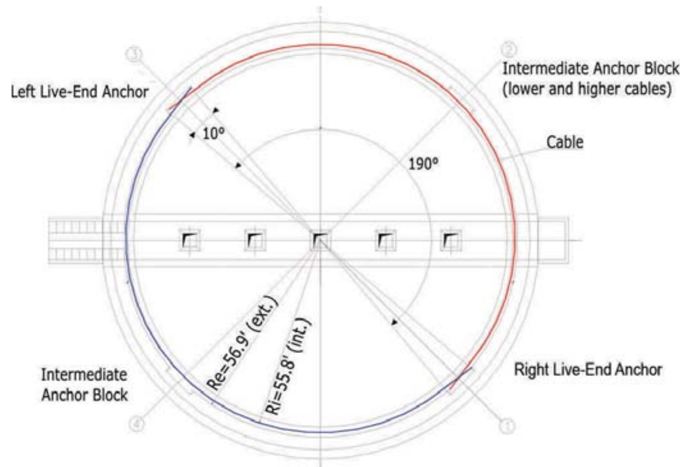

Fig. 6—Clinker silo plan view.

point is in a fixed position at the fixed end anchor. Moreover, the elongation related to the current post-tensioning step can be simply derived as the difference between the total elongation of the current tensioning step and that of the previous total one.

Finally, if the tensioning procedure is equalized as previously described, the total elongation of the tendon at the end of the k-th equalized step then becomes ($L = R\theta_o$)

$$\Delta L_{K,eq,tot} = \frac{N_K L}{EA}\left[\frac{1-e^{-\mu\vartheta_o/2}}{\mu\vartheta_o/2}\right] \quad (17)$$

CASE STUDY

The post-tensioning of the cylindrical wall of the silo storing clinker pictured in Fig. 5 is analyzed. The wall has an inner radius of 55.8 ft (17.0 m) and a thickness of 13.8 in. (35 cm). It is post-tensioned by means of 32 pairs of semicircular tendons placed at two-thirds of the thickness of the wall that extend between opposite blocks. The

Table 1—Clinker silo: tendon geometric and mechanical data

R	56.6 ft (17.25 m)
θ_o	190 degrees (3.316 rad)
E	29×10^6 psi (200,000 N/mm^2)
A	2.58 in.^{2} (1668 mm^2)
$N1$	157 kip (700 kN)
$N2$	337 kip (1500 kN)
$N3$	517 kip (2300 kN)

tendons are alternated along the height of a wall 105 ft (32.0 m) high. Each tendon is composed of twelve 0.6 in. (15.2 mm) steel strands whose main parameters are collected in Table 1 (A = 2.58 in.^{2} [16.68 cm^2]; E = 29.0 × 10^6 psi (200,000 MPa); and R_{cables} = 56.6 ft [17.25 m]). All the steel strands are placed inside steel ducts, which are grouted after the tensioning of the tendons. The angular width of the tendons is 190 degrees (3.316 rad) and their length is 188 ft (57.2 m), as shown in Fig. 6. The tendons apply, operating from two opposite block anchors (Fig. 7) in 3+3 equalized steps of 157, 180, and 180 kip (700, 800, and 800 kN)—a total prestressing force N_{eq} = 517 kip (2300 kN)—which ensures to counterbalance the outward pressure exerted by the weight of the clinker.

BACK ANALYSIS OF MEASURES OF ELONGATIONS

For the clinker silo of this case study, the average values of the measured cumulative elongations of the tendons in the six prestressing steps were found to be 3.15, 3.70, 6.73, 8.11, 10.83, and 12.52 in. (8.0, 9.4, 17.1, 20.6, 27.5, and 31.8 cm), as shown in Table 2 (1.0 in. = 2.54 cm). The 517 kip (2300 kN) total prestressing force was applied in three equalized steps, increasing the prestressing force up to 157, 337, and 517 kip (700, 1500, and 2300 kN) following a step-by-step procedure. The force was increased to the next prestressing value only when all the tendons of the silo were post-tensioned at the same current prestressing force. The experimental measures of the elongations of the tendons were processed by means of the equations found previously, collected and converted to inches in Tables 3 and 4. It was possible to calculate the value of the total friction coefficient, which also includes the wobble effect, finding

$$\hat{\mu} = 0.28 \tag{18}$$

Considering that the wobble coefficient κ is a measure of the unintentional local misalignment,[4] the total friction losses along an arc of the tendon can be written as the sum of the curvature friction loss ($\mu \cdot \theta$) and of the wobble friction loss ($\kappa \cdot s$), with $s = R\theta$—the length of the arc. This criterion[5,6] establishes the following equivalence in terms of friction losses for a current point along the tendon

$$N_T \cdot e^{-\hat{\mu} \cdot \vartheta} = N_T \cdot e^{-(\mu \cdot \vartheta + \kappa \cdot s)} \tag{19}$$

which provides

$$\hat{\mu} \cdot \vartheta = \mu \cdot \vartheta + \kappa \cdot s \tag{20}$$

Assuming the wobble coefficient to be $\kappa = 0.0006$ rad/ft ($\kappa = 0.002$ rad./m) as indicated by Hewson,[7] one can estimate through a back-analysis value of the curvature friction coefficient, finding

$$\mu = \hat{\mu} - \kappa \cdot R \cong 0.25 \tag{21}$$

This value agrees with those provided for the steel strands inside steel ducts by the main international codes of practice, such as the Eurocode EC2-EN-1992-1-1.[8]

INTERPRETATION OF RESULTS AND COMPARISON

An example of the application of the algorithm in the interpretation of the back-analysis results of the case study and in the comparison between the two cases of low and high friction is illustrated herein. The evaluation of the total elongations of the tendons is shown first for the case of greased and plastic-sheathed strands for which $\mu = 0.10$. Then, the case of the tendon design of the clinker silo in which the steel strands are placed inside steel ducts and then grouted is analyzed assuming, as shown, $\mu = 0.28$.

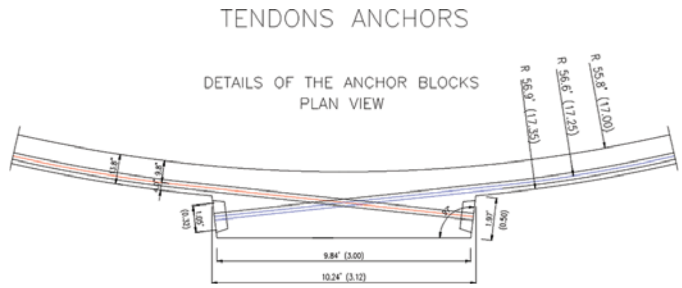

Fig. 7—Anchor block details.

Table 2—Back-analysis correlation between forces at live ends and elongation of tendons (μ = 0.28)

Step No.	Live end anchor	N, kip (kN)	ΔL_{theor} (μ = 0.28), in. (cm)	ΔL_{exp}, in. (cm)
1	Right	157 (700)	3.07 (7.8)	3.15 (8.0)
2	Left	157 (700)	3.77 (9.6)	3.70 (9.4)
3	Right	337 (1500)	6.61 (16.8)	6.73 (17.1)
4	Left	337 (1500)	8.11 (20.6)	8.11 (20.6)
5	Right	517 (2300)	10.67 (27.1)	10.83 (27.5)
6	Left	517 (2300)	12.44 (31.6)	12.52 (31.8)

The diagram illustrating the total elongations of the tendons as a function of the force at the live end is shown in Fig. 8 for the case of greased and plastic-sheathed strands ($\mu = 0.10$). Due to the low value of the friction coefficient, the applied forces in the third and the fifth post-tensioning steps are high enough to produce the complete inversion of the friction forces along the tendon, as shown by the straight segments of the diagram. It can be noted that the length of the straight lines reduces as the applied force increases, confirming the fact that as the prestressing force is increased, more force is needed to overcome the growing friction resistance.

The diagram of the total elongations of the tendons as a function of the force at the live end for the case of steel strands placed inside steel ducts ($\mu = 0.28$) is shown in Fig. 9 while, in Fig. 10, the diagram of the correlation between the live end force and the angle that defines the position of the inversion point is shown. As a consequence of the higher friction coefficient, in the third and the fifth post-tensioning steps, there is not a complete inversion of the friction forces, and the efficiency of the prestress is reduced. The friction losses become relevant and the force applied at the fixed end anchor in the previous step remains unchanged. The successive step equalizes the end force,

Table 3—Clinker silo: measured tendon elongations (in.)—Tendon Path 1-3/3-1

Path a: Block 1 - Block 2 - Block 3, Path b: Block 1 - Block 4 - Block 3									
Tendon	Anchor Block No. 1				Anchor Block No. 3				Total
Family No.	1st step (160 kip) (700 kN)	3rd step (340 kip) (1500 kN)	5th step (520 kip) (2300 kN)	Total A	2nd step (160 kip) (700 kN)	4th step (340 kip) (1500 kN)	6th step (520 kip) (2300 kN)	Total B	A + B
31 a	3.15	2.56	2.56	8.27	0.59	1.38	1.77	3.74	12.01
31 b	3.15	2.95	2.95	9.06	0.59	1.57	1.57	3.74	12.80
29 a	3.15	3.35	2.56	9.06	0.39	1.77	1.18	3.35	12.40
29 b	3.15	2.36	2.36	7.87	0.59	1.77	1.57	3.94	11.81
27 a	3.15	2.76	2.56	8.46	0.39	1.77	1.57	3.74	12.20
27 b	3.15	2.76	2.56	8.46	0.59	1.57	1.77	3.94	12.40
25 a	3.15	2.95	2.56	8.66	0.39	1.38	1.97	3.74	12.40
25 b	3.15	3.15	2.56	8.86	0.59	1.18	1.97	3.74	12.60
23 a	3.15	2.76	3.35	9.25	0.59	1.38	1.38	3.35	12.60
23 b	3.15	3.35	2.76	9.25	0.59	1.57	1.77	3.94	13.19
21 a	3.15	2.76	2.95	8.86	0.59	1.38	1.38	3.35	12.20
21 b	3.15	2.95	2.76	8.86	0.59	1.57	1.57	3.74	12.60
19 a	3.15	3.15	2.76	9.06	0.59	1.18	1.97	3.74	12.80
19 b	3.15	3.15	2.76	9.06	0.39	1.38	1.77	3.54	12.60
17 a	3.15	2.95	2.56	8.66	0.39	1.18	1.77	3.35	12.01
17 b	3.15	2.95	2.76	8.86	0.39	1.38	1.77	3.54	12.40
15 a	3.15	3.15	2.76	9.06	0.39	0.98	1.97	3.35	12.40
15 b	3.15	2.95	2.95	9.06	0.39	1.18	1.77	3.35	12.40
13 a	3.15	2.95	2.56	8.66	0.59	1.38	2.17	4.13	12.80
13 b	3.15	2.76	2.56	8.46	0.39	1.38	1.77	3.54	12.01
11 a	3.15	2.95	2.76	8.86	0.59	1.57	1.77	3.94	12.80
11 b	3.15	2.95	2.76	8.86	0.59	1.18	1.77	3.54	12.40
9 a	3.15	2.95	2.76	8.86	0.59	1.18	1.97	3.74	12.60
9 b	3.15	2.95	2.95	9.06	0.39	1.38	2.17	3.94	12.99
7 a	3.15	3.15	2.56	8.86	0.39	1.38	1.77	3.54	12.40
7 b	3.15	3.35	2.95	9.45	0.39	1.38	1.77	3.54	12.99
5 a	3.15	2.95	2.56	8.66	0.59	1.77	1.57	3.94	12.60
5 b	3.15	2.95	2.17	8.27	0.59	1.57	1.97	4.13	12.40
3 a	3.15	2.76	2.56	8.46	0.39	1.38	1.57	3.35	11.81
3 b	3.15	2.36	2.36	7.87	0.59	1.57	1.77	3.94	11.81
1 a	3.15	2.56	2.76	8.46	0.59	1.77	1.57	3.94	12.40
1 b	3.15	2.95	2.56	8.66	0.59	1.38	1.77	3.74	12.40

Note: 1 in. = 25.4 mm.

leading to a symmetric distribution of the axial forces in the tendon, which reaches its minimum in the middle of the tendon in front of the intermediate blocks, where its value is lesser then that of the previous case.

The distribution of the axial force along the tendon, computed using the back-analysis value of the friction coefficient $\mu = 0.28$, is illustrated in Fig. 11. This diagram shows that the sum of the area, A_i ($i = 1, 2,..., 6$), under the curve for each single tensioning step (which is proportional to the term R/EA of the specific step elongation of the tendon), gives the same total area as if the final equalized tensioning was done in a single step acting simultaneously

Table 4—Clinker silo: measured tendon elongations (in.)—Tendon Path 2-4/4-2

Path a: Block 2 - Block 3 - Block 4; Path b: Block 2 - Block 1 - Block 4									
Tendon	Anchor Block No. 2				Anchor Block No. 4				Total
Family No.	1st step (160 kip) (700 kN)	3rd step (340 kip) (1500 kN)	5th step (520 kip) (2300 kN)	Total A	2nd step (160 kip) (700 kN)	4th step (340 kip) (1500 kN)	6th step (520 kip) (2300 kN)	Total B	A + B
32 a	3.15	2.76	2.36	8.27	0.59	1.18	1.77	3.54	11.81
32 b	3.15	2.76	2.36	8.27	0.59	1.38	1.77	3.74	12.01
30 a	3.15	3.35	2.56	9.06	0.39	1.18	1.77	3.35	12.40
30 b	3.15	3.15	2.76	9.06	0.39	1.57	1.97	3.94	12.99
28 a	3.15	3.15	3.15	9.45	0.59	1.18	1.57	3.35	12.80
28 b	3.15	2.95	2.76	8.86	0.59	1.38	1.97	3.94	12.80
26 a	3.15	3.15	2.76	9.06	0.59	0.98	1.77	3.35	12.40
26 b	3.15	2.76	2.36	8.27	0.59	1.18	1.97	3.74	12.01
24 a	3.15	3.35	2.76	9.25	0.59	1.38	1.97	3.94	13.19
24 b	3.15	3.15	2.56	8.86	0.59	1.38	1.97	3.94	12.80
22 a	3.15	3.94	2.95	10.04	0.59	1.38	1.18	3.15	13.19
22 b	3.15	3.35	2.95	9.45	0.39	1.38	1.18	2.95	12.40
20 a	3.15	3.35	2.95	9.45	0.59	1.18	1.18	2.95	12.40
20 b	3.15	3.74	2.95	9.84	0.59	1.18	1.38	3.15	12.99
18 a	3.15	3.15	3.15	9.45	0.59	1.38	1.57	3.54	12.99
18 b	3.15	3.35	2.95	9.45	0.39	1.38	1.18	2.95	12.40
16 a	3.15	3.35	3.35	9.84	0.59	0.79	1.57	2.95	12.80
16 b	3.15	2.95	2.95	9.06	0.59	0.79	1.77	3.15	12.20
14 a	3.15	2.95	2.95	9.06	0.59	0.79	1.77	3.15	12.20
14 b	3.15	3.15	2.95	9.25	0.59	1.38	1.77	3.74	12.99
12 a	3.15	3.15	2.95	9.25	0.59	1.18	1.57	3.35	12.60
12 b	3.15	2.76	2.56	8.46	0.59	1.77	1.97	4.33	12.80
10 a	3.15	3.15	2.56	8.86	0.59	1.38	1.57	3.54	12.40
10 b	3.15	2.76	2.56	8.46	0.39	1.38	1.97	3.74	12.20
8 a	3.15	3.54	2.95	9.65	0.59	1.18	1.38	3.15	12.80
8 b	3.15	3.74	3.15	10.04	0.39	1.18	1.18	2.76	12.80
6 a	3.15	3.15	2.95	9.25	0.59	1.57	1.18	3.35	12.60
6 b	3.15	3.35	2.95	9.45	0.59	1.18	1.38	3.15	12.60
4 a	3.15	3.35	2.36	8.86	0.59	1.38	1.57	3.54	12.40
4 b	3.15	2.95	2.76	8.86	0.59	1.38	1.38	3.35	12.20
2 a	3.15	2.95	2.76	8.86	0.39	1.57	1.18	3.15	12.01
2 b	3.15	3.35	2.36	8.86	0.59	1.38	1.77	3.74	12.60

Note: 1 in. = 25.4 mm.

from both ends (Fig. 12). As a consequence, the same total elongation is calculated. In this case, the position of the inversion point is clamped at the fixed end anchor in the first tensioning step at 157 kip (700 kN), at the intersection of the Curves A2-A3 at the first tensioning at 337 kip (1500 kN), and of Curves A4-A5 at the first tensioning at 517 kip (2300 kN). It is instead placed at the intersection between Curves A1-A2, A3-A4, and A5-A6 at the middle length of the tendon at the end of each of the three equalizing steps. The resulting distribution of the average value of the post-tensioning axial forces provided by the upper level and the lower level of the circular tendons, which are

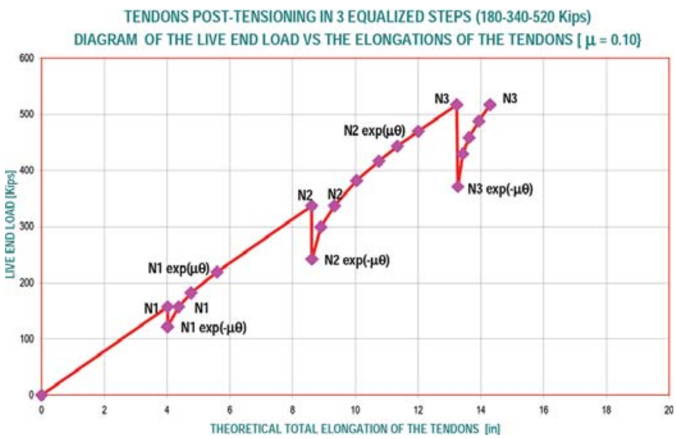

Fig. 8—Tendon post-tensioning in three equalized steps (μ = 0.10).

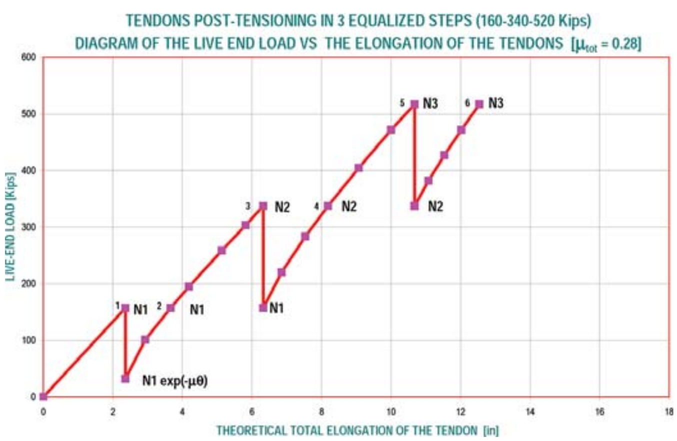

Fig. 9—Tendon post-tensioning in three equalized steps (μ = 0.28).

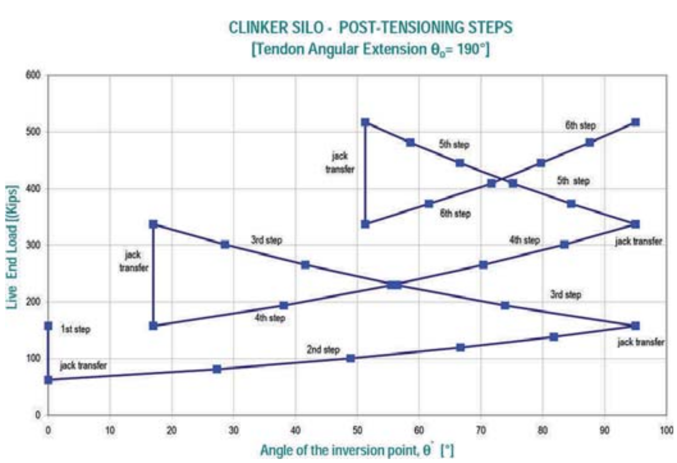

Fig. 10—Correlation between live end load and position of inversion point (μ = 0.28).

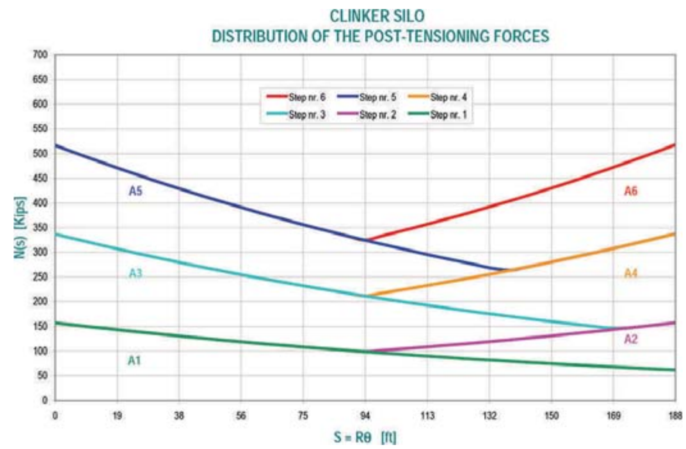

Fig. 11—Distribution of axial forces in post-tensioning steps (μ = 0.28).

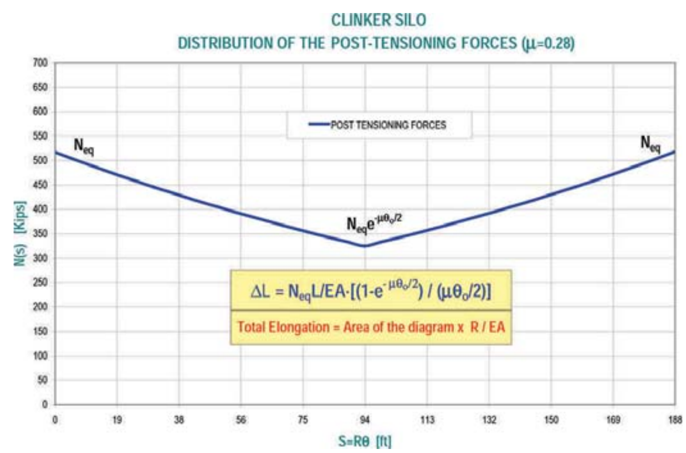

Fig. 12—Distribution of axial forces in tendon at final equalized steps (μ = 0.28).

anchored in blocks built 90 degrees apart, is illustrated in Fig. 13. The uniformity of the prestress along the wall is reached as a resulting effect provided by the tensioning of two consecutive families of tendons. The value of the average axial force can be estimated considering that the total elongations given by Eq. (17) are that of an equivalent tendon tensioned with a constant force equal to

$$N_{ave} = N_{eq} \cdot \left[\frac{1 - e^{-\mu\vartheta_o/2}}{\mu\vartheta_o/2} \right] \qquad (22)$$

The term inside the brackets of Eq. (22) thus provides a synthetic evaluation of the efficiency of the prestress operation at the end of the equalized post-tensioning step. In the case study, the value of that efficiency is 80%.

Finally, the measured and the back-analysis curves of the elongation of the tendon as a function of the tensioning step are illustrated in Fig. 14 together with the elongation of the tendon in the case in which no friction acts. The comparison between these curves gives a direct view of the growing influence of the frictional losses as the applied post-tensioning forces increase.

CONCLUSIONS

In this paper, the step-by-step post-tensioning of cylindrical shells was analyzed with the purpose of evaluating the distribution of the axial force and the elongations of the tendons. It was found is that it is possible to identify, for any value of the applied prestressing force at the live end anchor, a characteristic point along the tendon in which the displacement of the tendon in the current prestressing step is zero. Such a point divides the tendon in two segments; in the first one, the friction forces invert with respect to the applied tensioning force (and in which segment the strands stretch) from a second one, in which the distribution of the axial force induced by the previous tensioning step remains unchanged (and in which segment the strands remain in the duct without slip). This behavior occurs especially when the step-by-step stressing is applied with the same prestressing force at both ends of the tendon. The multi-step stressing of post-tensioning tendons is desirable when using steel strands placed inside steel ducts in very long tendons or when the curvature of the tendon is significant. In any case, the distribution of the axial force and the elongation of the tendons can be found by means of simple analytical formulas that can be easily implemented in an electronic spreadsheet. That allows one to compare the measured elongations to the design parameters, providing the synthesis of control of the post-tensioning operations.

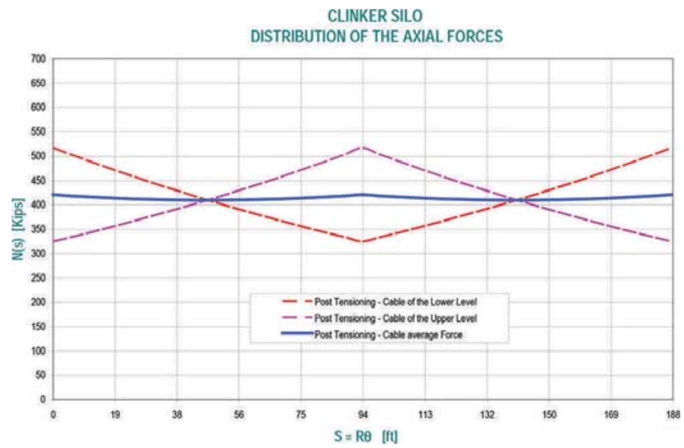

Fig. 13—Diagram of distribution of average axial forces ($\mu = 0.28$).

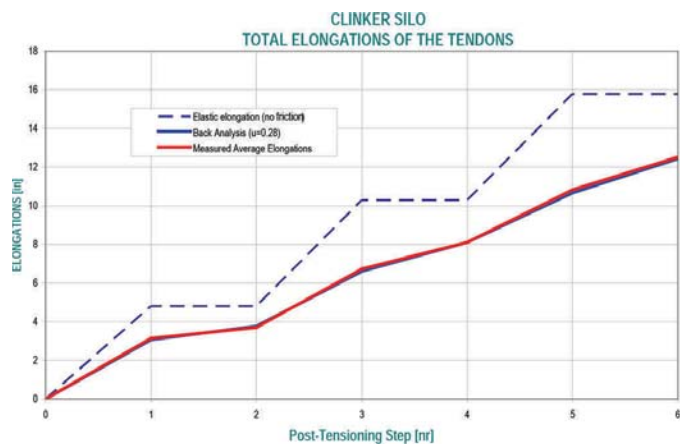

Fig. 14—Step-by-step diagram of total elongation of tendons ($\mu = 0.28$).

NOTATION

A = area of cross section of strands in tendon
b = thickness of cylindrical shell
E = elastic modulus of strand
H = height of cylindrical shell
L = length of tendon
L_L = length of tendon at left side of inversion point
L_R = length of tendon at right side of inversion point
N = axial force in current point of tendon
N_{eq} = equalized prestressing force
N_F = prestressing force acting at dead end anchor
N_K = prestressing force applied in current post-tensioning step
N_L = prestressing force acting at left anchor
N_R = prestressing force acting at right anchor
N_T = prestressing force acting at live end anchor
p = contact pressure
R = radius of tendon
s = curvilinear coordinate
t = friction force
u = axial displacement
ΔL = elongation of tendon
δ = slip between strands and duct
κ = wobble friction coefficient
μ = curvature friction coefficient
θ = angle of current point along tendon
θ^* = angle of inversion point
θ_o = angular width of tendon

REFERENCES

1. Cestelli Guidi, C., *Prestressed Reinforced Concrete*, U. Hoepli, ed., Milan, Italy, 1974.

2. Antonini, T., *Prestressed Reinforced Concrete*, CLUP, ed., Milan, Italy, 1978.

3. Lin, T. Y., and Burns, N. H., *Design of Prestressed Concrete Structures*, Wiley, New York, 1981, 646 pp.

4. Goffi, L., and Marro, P., *Notebook on Prestressed Concrete*, CLUT, Turin, Italy, 1998.

5. Pozzo, E., *The Prestressed Reinforced Concrete*, V. III, Pitagora, ed., Bologna, Italy 1999.

6. Nawy, E. G., *Prestressed Concrete: A Fundamental Approach*, Prentice Hall, New York, 2000, 938 pp.

7. Hewson, N., *Prestressed Concrete: Design and Construction*, Thomas Telford, London, UK, 2003, 371 pp.

8. Eurocode 2, "EC 2-EN 1992-1-1, Design of Concrete Structures. Part 1-1: General Rules and Rules for Buildings," European Committee for Standardization, Brussels, Belgium, 2005.

Maurizio Lenzi *is Technical Director of the Cooperative ACMAR of Ravenna, Italy, where he works as a Structural Designer. He graduated from the University of Bologna, Bologna, Italy, in 1982. His research interests include post-tensioned bridges and slabs, retrofit of bridges by means of carbon fiber-reinforced polymer (CFRP) post-tensioning, cable-stayed bridges, tanks, silos, and wharves restrained by post-tensioned underwater anchors.*

Paola Campana *is a Consulting Engineer at a firm in Forli, Italy. She graduated from the University of Bologna in 1994. Her research interests include geotechnics, the structural design of pile foundations, slurry walls, tiebacks, marine construction, post-tensioned underwater anchors, retrofit of structures with CFRP materials, and the strengthening of bridges by means of the post-tensioning of CFRP plates.*